NANO · MICRO small
www.small-journal.com

Atomically Dispersed Heteronuclear Dual-Atom Catalysts: A New Rising Star in Atomic Catalysis

Tianwei He, Alain R. Puente Santiago, Youchao Kong, Md Ariful Ahsan, Rafael Luque,* Aijun Du,* and Hui Pan**

Atomic catalysts (AC) are gaining extensive research interest as the most active new frontier in heterogeneous catalysis due to their unique electronic structures and maximum atom-utilization efficiencies. Among all the atom catalysts, atomically dispersed heteronuclear dual-atom catalysts (HDACs), which are featured with asymmetric active sites, have recently opened new pathways in the field of advancing atomic catalysis. In this review, the up-to-date investigations on heteronuclear dual-atom catalysts together with the last advances on their theoretical predictions and experimental constructions are summarized. Furthermore, the current experimental synthetic strategies and accessible characterization techniques for these kinds of atomic catalysts, are also discussed. Finally, the crucial challenges in both theoretical and experimental aspects, as well as the future prospects of HDACs for energy-related applications are provided. It is believed that this review will inspire the rational design and synthesis of the new generation of highly effective HDACs.

1. Introduction

Energy crisis and global climate change are the two big pressing problems nowadays that endow researchers to seek effective strategies to deal with them.[1–3] Renewable energy conversion technologies provide a sustainable and green route to address these urgent issues.[4,5] Water splitting, nitrogen fixation or carbon dioxide reduction, which can also be driven by clean and renewable energies such as wind, solar and hydropower resources, represent crucial steps of these renewable energy devices. However, the performances of these chemical reactions strongly rely on the energy storage and conversion efficiencies of the catalytic materials deposited on the electrodes.[6–10] Therefore, the development of robust and earth-abundant catalysts with both high catalytic activity and selectivity play a critical role in the real application of these devices.

Current catalysts for energy-related chemical reactions are heavily dependent on noble metals, which impedes their large potential commercialization.[11–13] Further, the catalytic process mostly occurred on the metal surfaces, leading to the very low utilization efficiency of the catalysts. To minimize the waste of the non-accessible atoms in the bulk metals, researchers developed several strategies to modify metal structures in order to expose as many metal atoms as possible.[10,14–18] One of the most popular methods is to downsize the solid metal catalysts to the atomic level (**Figure 1**). More interestingly, the catalytic behaviors of the metal catalysts with different sizes have significantly

T. He, Y. Kong, H. Pan
Institute of Applied Physics and Materials Engineering
University of Macau
Macao SAR 999078, P. R. China
E-mail: huipan@um.edu.mo

T. He
Fritz-Haber-Institut
Max-Planck-Gesellschaft zur Förderung der Wissenschaften e.V.
Theory Department
Faradayweg 4-6, 14195 Berlin, Germany
E-mail: the@fhi.mpg.de

A. R. P. Santiago, M. A. Ahsan
Department of Chemistry
University of Texas at El Paso
500 West University Avenue, El Paso, TX 79968, USA

The ORCID identification number(s) for the author(s) of this article can be found under https://doi.org/10.1002/smll.202106091.

DOI: 10.1002/smll.202106091

R. Luque
Department of Organic Chemistry
University of Cordoba
Campus de Rabanales, Edificio Marie Curie (C-3), Ctra Nnal IV-A, Km 396, Cordoba E14014, Spain
E-mail: rafael.luque@uco.es

R. Luque
Russia Centre for Materials Science and School of Chemistry and Physics
Peoples Friendship University of Russia (RUDN University)
6 Miklukho-Maklaya str, Moscow 117198, Russian Federation

A. Du
Queensland University of Technology
Garden Point Campus
Brisbane, Queensland 4001, Australia
E-mail: aijun.du@qut.edu.au

H. Pan
Department of Physics and Chemistry
Faculty of Science and Technology
University of Macau
Macao SAR 999078, P. R. China

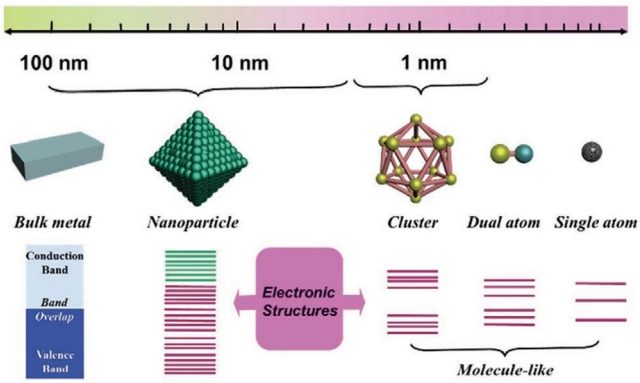

Figure 1. The geometric and electronic structures for bulk metal, nanoparticle, cluster, dual atom, and single atom materials. Reproduced with permission.[10] Copyright 2020, Royal Society of Chemistry.

changed due to the altered coordinated environment of the active sites. Well-defined active sites with tunable electronic structures are currently making the atomic catalysts a hot frontier in a variety of chemical reactions.[19–21] For example, since the first synthesized single Pt atom anchored on FeO_x support by Zhang's group in 2011,[22] single atom catalysts (SACs) have emerged as the brightest stars in heterogeneous catalysis. The 100% atomic utilization and finely dispersed active sites leave a lot of room for rational design and synthesis of specific catalysts.[23–30] Despite the outstanding properties of SACs, there are various restrictions for these kinds of single-atomic structures, which hold back their further development.[31,32] One of the largest limitations is the only one isolated atom that may suffer from insufficient adsorption sites in some reactions that involve co-adsorption of multiple reactants.[33–36] An effective strategy to address this problem is the introduction of another isolated atom to form dual active sites, namely the dual-atom catalysts (DACs). In recent years, the exploration of DACs has received tremendous attraction owing to their great potential to enhance catalytic performance.[37–42] The isolated adjacent active sites can not only provide two adsorption sites but can also work synergistically to greatly promote the catalytic activity and selectivity. The current study of DACs is mainly focused on the homonuclear dual-atom catalysts, such as the Fe_2, Pt_2, Co_2 supported on graphene,[43–45] Pt_2 doped on MoS_2,[46] and Cu atom-pair anchored alloy nanowires.[33] The heteronuclear dual-atom catalysts (HDACs) that possess asymmetric active sites and demonstrate superior catalytic behaviors than those of homonuclear dual-atom catalysts have been gradually coming into the researchers' vision. This asymmetric active site defines as a dimer that exists on some form of support whereby each of the individual atoms is a different element. Compared to the symmetric homonuclear dimer active sites, these kinds of symmetry-breaking active centers could bring unique structure and electronic properties, such as a prominent charge density gradient in its active sites and a local torque that can enable more effective overlapping of atomic orbitals when activating the linear molecules. Meanwhile, the transition state on asymmetric dual active site differs from SACs that may break the traditional linear scaling, giving ample design space while the latter can only modify electronic states of one active atom. All these properties surpass the benefits of the SACs and homonuclear dual-atom catalysts, and also their unique advantages of the symmetry-breaking sites toward activating small molecules, such as N_2, CO, CO_2, and H_2O, are highly desirable.

Actually, such kind of asymmetric active centers has already appeared in many catalytic reactions. Gong et al.[47] synthesized 1-nm-thick Pt_3Ni bimetallic alloy nanowires with enhanced activity and durability for oxygen reduction reaction due to the structural advantages of PtNi composition. Hu et al.[48] prepared a novel PtCo@NC catalyst with different Pt—Co biatomic arrangements, thus achieving a remarkable enhanced electrocatalytic performance for the methanol oxidation reaction. The results reveal that the improved activity is attributed to the reorganization of the electron distribution around the Pt/Co active centers, which facilitated the formation of O*. Moreover, the isolation of a single metal atom on another metal surface to form surface alloys has also been verified to be the benefit of the catalytic reactivity.[49] Zhao's group[50] reported Cu—Sn single-atom surface alloys that enable distinct catalytic selectivity for CO_2 reduction due to the unique geometric and electronic structure of Cu–Sn surface alloys. Further, Chen et al.[51] constructed a copper–ceria interfacial structure by loading a copper cluster on the oxygen vacancies of ceria for the water–gas shift reaction. The active sites are identified as the cooperated Cu–Ce atoms at the interfacial in which the Cu site chemically adsorbs CO, whereas the Ce site activates H_2O. Although the above experiments suggest that heteronuclear dual-atom active sites exhibit enhanced catalytic performance, the activity and selectivity still need to be further improved. Interestingly, by isolating heteronuclear dual-atom active sites, namely the atomically dispersed heteronuclear dual-atom sites, the catalytic performance can be greatly boosted. Whereas the recent investigations on both theoretical and experimental of atomically dispersed heteronuclear dual-atom catalysts (HDACs) are still in its initial stage, the great potential for achieving higher catalytic performance of HDACs has sparked the attention of the catalysis community.

In this review, we introduce the latest theoretical studies on the nature of HDACs, including the comparison of their reaction mechanisms with the homonuclear dual-atom pair. The theoretical predictions of the HDACs in various catalytic reactions are also provided. Next, the state-of-the-art experimental syntheses, characterizations, and energy-related applications of HDACs are summarized and discussed. Finally, an outlook on such a burgeoning direction in atomic catalysis is presented.

2. Theoretical Exploration of HDACs

Unlike the single atom and homonuclear dual-atom catalysts, HDACs possess a pair of asymmetric active sites that provide them unique catalytic behaviors. HDACs can form a bridge between SACs and homonuclear dual-atom catalysts by taking advantage of both of them. First, the additional active site is very suitable to catalyze a more complicated catalytic process that involves multiple reaction steps and intermediates. Second, the two different kinds of atoms form asymmetric active sites, which could activate linear molecules (such as CO_2) as well as potentially break the traditional linear scaling relationship to overcome the kinetic energy barriers during the catalytic

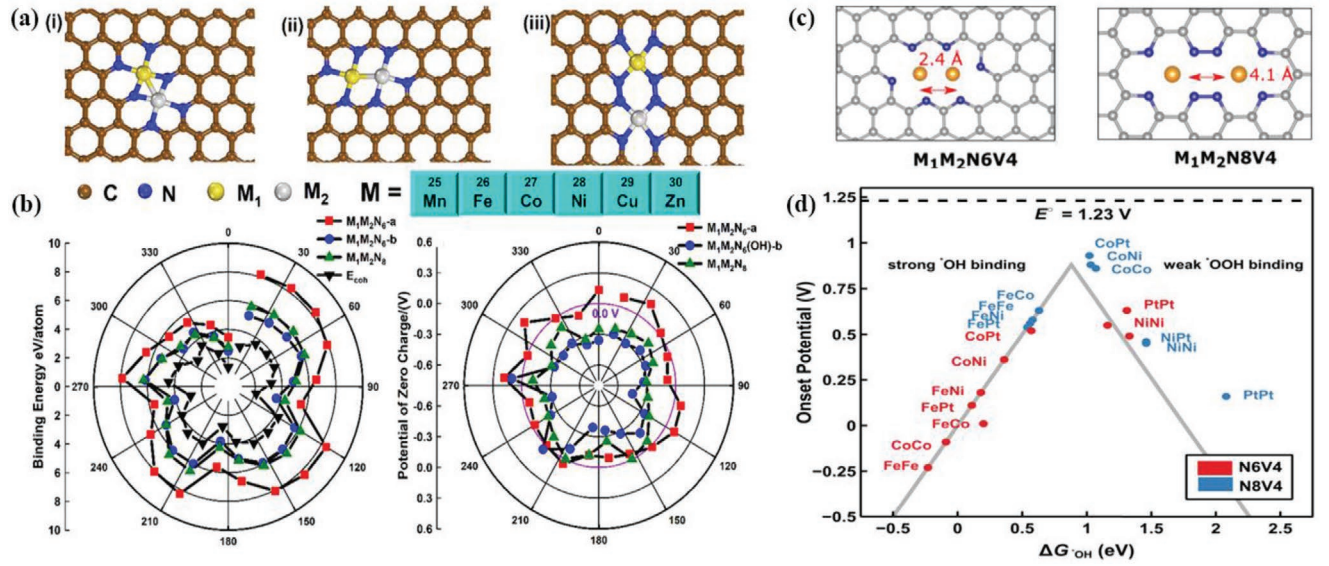

Figure 2. a) Three different configurations of dual-metal site catalyst models. b) The calculated average binding energy, cohesive energy, and potential of zero charge of the dual-metal atoms. Reproduced with permission.[54] Copyright 2021, Elsevier. c) The models of dual-metal atoms doped in two-atom (N_6V_4) and four-atom (N_8V_4) vacancy in graphene. d) The activity volcano map of ORR for $M_1M_2N_6V_4$ and $M_1M_2N_8V_4$. Reproduced with permission.[55] Copyright 2019, American Chemical Society.

reactions. Therefore, the studies of HDACs have recently attracted widespread interest in the catalysis community.

Thanks to the fast development of various theoretical approaches such as the density functional theory (DFT) calculations, microkinetic modeling, ab initio molecular dynamic (AIMD) simulations, and machine learning (ML), theoretical modeling plays a pivotal role in the prediction of new catalysts and the exploration of their reaction mechanisms. The multiple possibilities of combinations and difficulties in the accurate synthesis of atomically dispersed heteronuclear dual-atom catalysts make the theoretical modeling an essential and effective tool to screen out the most efficient candidates as well as explain the corresponding catalytic mechanisms.[52–54] However, as the same problem is faced with the SACs, the anchoring of the atomically dispersed asymmetric active sites on suitable substrates is the biggest challenge for their real and large-scale applications. In this section, we focus on the theoretical exploration of atomically dispersed asymmetric active sites that have been computationally constructed using different materials such as LD-nanomaterials (0 D, 1 D, and 2 D networks), metal oxides, and metallic organic frameworks (MOFs) as well as their possible applications in different electrocatalytic reactions.

2.1. Low-Dimensional Networks

2D materials are atomically thin and plain-layered structures with large specific surface areas. They provide a great potential to serve as substrates for anchoring dual-atom active sites. Among them, graphene is the most popular one to support metal atoms. Liu et al.[55] launched a computational study of Pt and Ru dimers supported on graphene for the alkaline hydrogen evolution reaction (HER) mechanism. They systematically compared Pt_2, Ru_2, and PtRu dimer supported on nitrogen-doped graphene and the results showed that PtRu dimer displayed the lowest hydrogen adsorption free energy of −0.07 eV. They discovered their own scaling relationship based on dissociative chemisorption energy of water scales linearly with the kinetic barrier can be a singular activity descriptor for metal dimer catalysts. Wang et al.[56] investigated the oxygen reduction reaction (ORR) process on different dual-metal–nitrogen–carbon (DM–N–C) catalysts. They built two $M_1M_2N_6$ and one $M_1M_2N_8$ models (M = Mn, Fe, Co, Ni, Cu, and Zn) with 63 active centers for acidic ORR (**Figure 2**a). The thermal stability of the catalysts was first evaluated by calculating the binding energies and the results indicated that most of the dual-metal sites are stable within the N-doped graphene layers (Figure 2b). They also revealed that the M_1M_2 antibonding center could facilitate the O—O bond cleavage and meanwhile mitigate the *OH removal issue, leading to very high catalytic activity. Hunter et al.[57] theoretically studied the catalytic efficiency of paired and single-atom catalysts for ORR by screening different transition metal pairs embedded in two kinds of N-doped four-atom vacancies, denoted as $M_1M_2@N_6V_4$ and $M_1M_2@N_8V_4$ as shown in Figure 2c. To screen out the promising candidates, they utilized the ORR scaling relations to obtain a volcano plot for the catalytic activity (Figure 2d). $CoPt@N_8V_4$ was found to be the ideal ORR catalyst with an overpotential of 0.3 V. Moreover, Zhao et al.[58] reported that the hydroxyl group modified bimetal ($(HO)_2$–M_1M_2 /DG, where M_1 and M_2 are Ni, Co, and Fe) atoms anchored on N-doped graphene networks exhibited much higher catalytic activity for both oxygen evolution reaction (OER) and ORR than bare metal atoms, which provides a new direction on improving the HDACs. The asymmetrical dual-metal dimer supported on N-doped graphene was further predicted to be active for ORR by other researchers.[59–62]

Electrochemical nitrogen reduction reaction is becoming a promising alternative to the Haber–Bosch process because it can

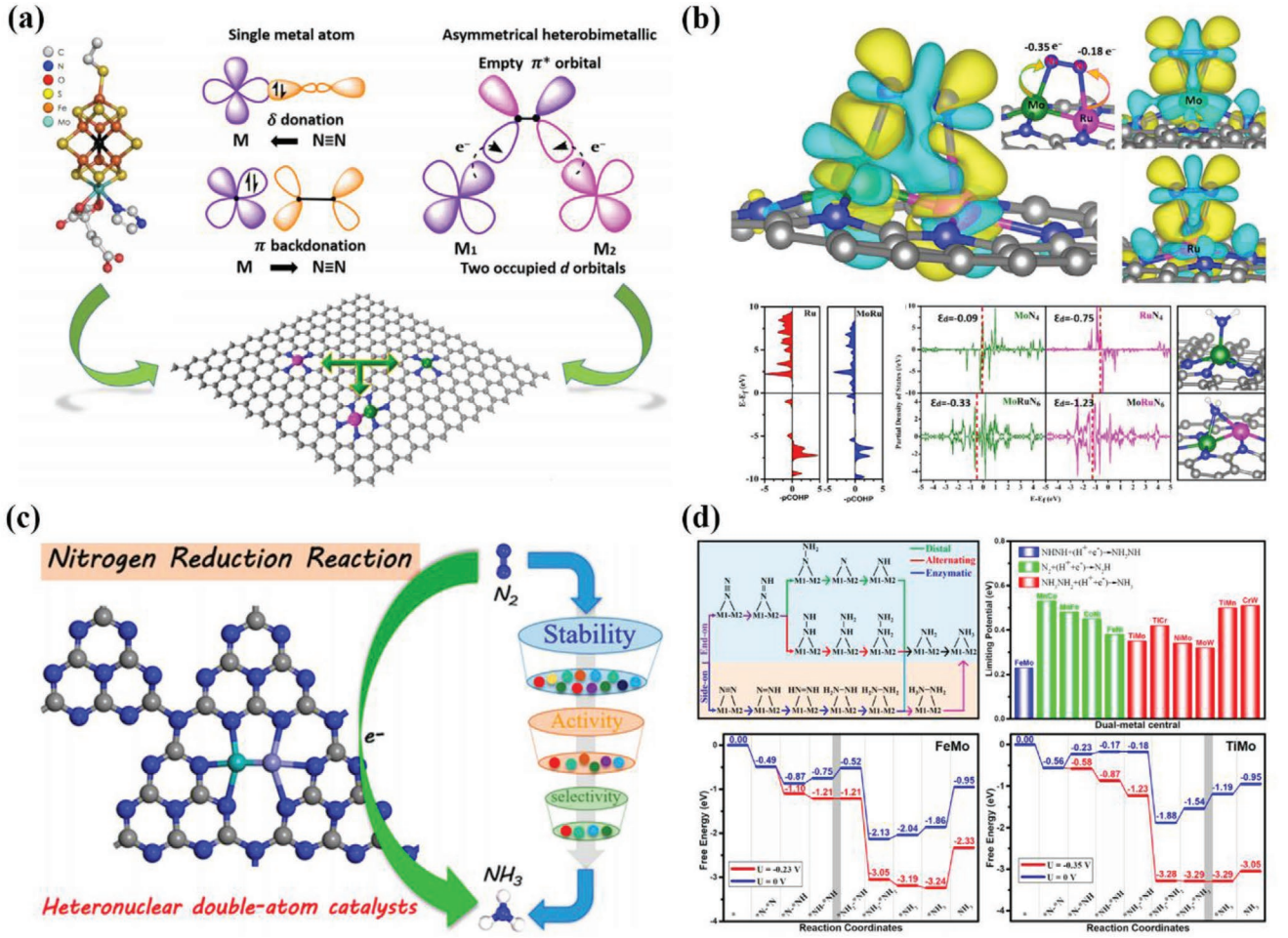

Figure 3. a) The design concept of asymmetric heteronuclear dual active sites for NRR. b) The reaction mechanism of NRR on asymmetrical dual-metal dimer catalytic center. Reproduced with permission.[62] Copyright 2020, Elsevier. c) The screening criteria for the high-throughput DFT calculation of heteronuclear double-atom catalysts for NRR. d) The reaction mechanisms and the most promising candidates for NRR. Reproduced with permission.[63] Copyright 2020, American Chemical Society.

be derived by sustainable energy under mild conditions.[63] However, the extremely high N≡N triple bond energy makes it very difficult to activate. He et al.[64] first theoretically proposed to use an asymmetrical dual-metal dimer catalytic center embedded in nitrogen-doped graphene framework ($M_1M_2N_6$-NG seeing in **Figure 3**a), which is inspired by the active sites of natural enzymes and can efficiently catalyze the reduction of N_2 to NH_3. They also unlocked the NRR mechanism on this kind of asymmetrical dual-metal dimer catalytic center (Figure 3b). The M_1 and M_2 metal atoms transferred different electrons to the two N atoms that can significantly polarize and weaken the N≡N bond. What's more, the two types of metal atoms can modify the d-band center of the corresponding single atom, leading to the moderate binding strength of the key intermediates. Porous 2D materials with abundant anchor sites, such as g-C_3N_4, C_2N, and graphdiyne, are excellent substrates for supporting dual-atom pairs. By using the stability, activity, and selectivity evaluation method. Wang et al.[65] screened out 16 effective heteronuclear dual-atom M_1M_2/g-C_3N_4 candidates for NRR (Figure 3c). They calculated all the three reaction pathways, including distal, alternating, and enzymatic mechanisms and summarized the potential determining step and limiting the potential of NRR on M_1M_2/g–C_3N_4 catalysts (Figure 3d). Among them, FeMo/g-C_3N_4 and TiMo/g-C_3N_4 were calculated as the most active electrocatalysts with particularly low limiting potentials of –0.23 and –0.35 V, respectively. Guo et al.[66] used large-scale DFT calculations to investigate 900 kinds of metal dimers supported on 2D expanded phthalocyanine (Pc). They constructed an activity map by using the N2H* adsorption as the descriptor and found 28 heteronuclear and 3 homonuclear highly efficient biatom catalysts. They also found that the heteronuclear catalysts can break the metal-based activity benchmark, leading to very high catalytic performances. Owing to the excellent catalytic performance, HDACs are widely investigated for NRR.[67–71] Similar to NRR, CO_2 activation and reduction is also very difficult due to the seriously restricted scaling relations. Ouyang et al.[72] designed heteronuclear transition-metal dimers supported on monolayer C_2N as effective dual-atom catalysts to break the scaling relations during CO_2RR. By comparing the metal surfaces and heteronuclear dual-atom active sites, they indicated

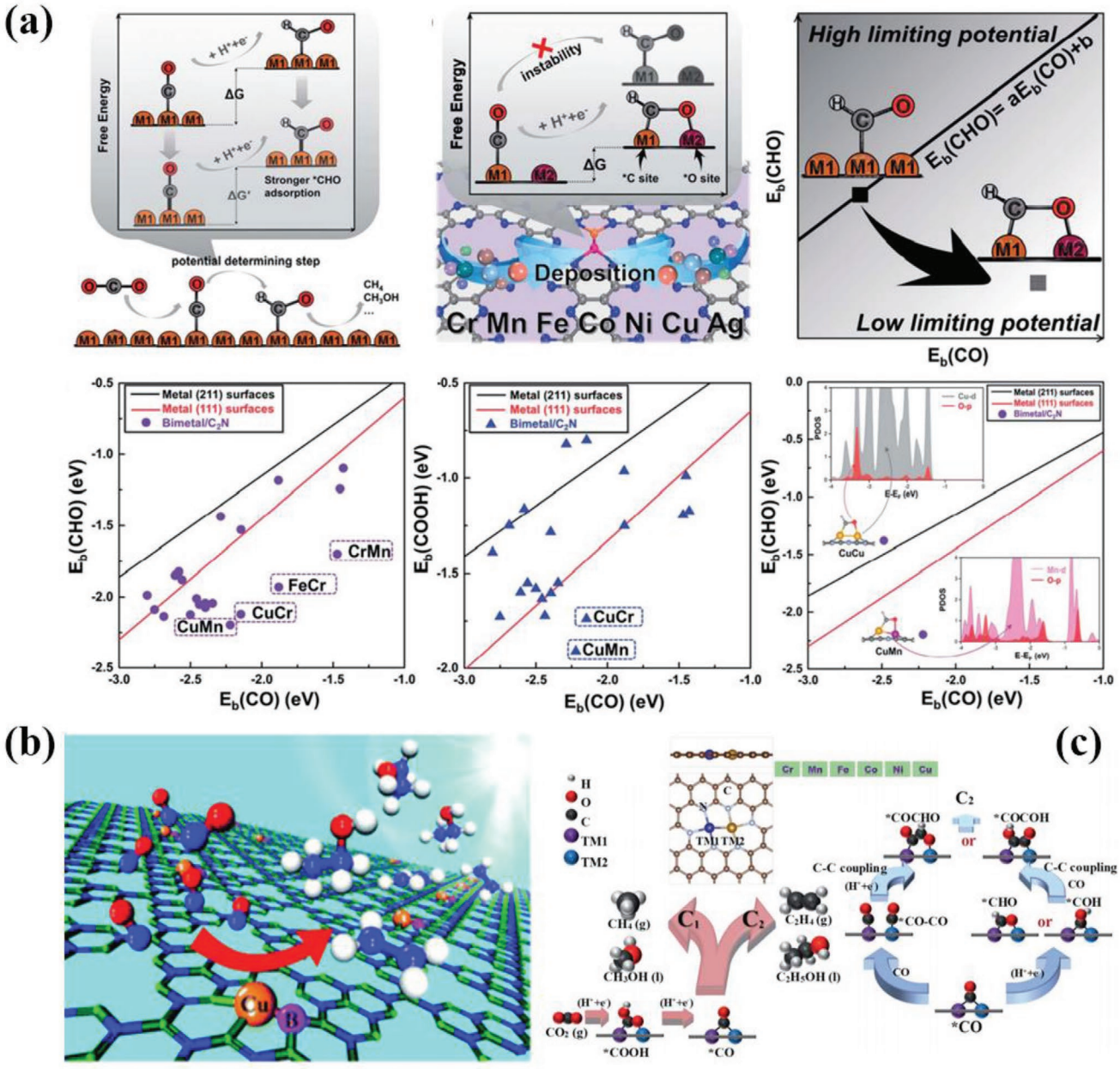

Figure 4. a) The scaling relations of intermediates on metal surfaces and the design concept of decoupling the scaling relations on asymmetrical dual-metal active sites. Reproduced with permission.[72] Copyright 2020, Royal Society of Chemistry. b) The structures of atomically dispersed metal and nonmetal catalytic center for CO reduction reaction. Reproduced with permission.[73] Copyright 2020, Royal Society of Chemistry. c) The reaction mechanism of CO_2 reduction to C_1 and C_2 products. Reproduced with permission.[75] Copyright 2020, Royal Society of Chemistry.

that the two different metal atoms could act as C-affinity and O-affinity binding sites, respectively, leading to a deviation from the transition-metal scaling relations (**Figure 4**a). Finally, CuCr/C_2N and CuMn/C_2N were selected out to be the most promising candidates for CO_2RR. The two active sites of HDACs can catalyze CO/CO_2 into C_{2+} products. Unlike the dual-metal atoms, He et al.[73] first reported isolated Cu–B atomic pairs anchored on g-C_3N_4 as a highly active photocatalyst for the conversion of CO into C_2 products (Figure 4b). The low-coordinated Cu–B active site and the synergistic of metal and nonmetal d–p coupling can significantly decrease the CO dimerization barrier. This work highlighted a new concept toward the synergistic coupling between metal and non-metal atoms, which had also been used to construct metal and no-metal interface as highly effective active sites for chemical reactions.[74] Similar work was also conducted and verified by Li et al.[75] that reported Co–B dimer anchored in C_2N could boost the C—C coupling to C_{2+} products. Chen et al.[76] conducted a systematic computational screening of DACs for CO_2RR to C_2H_5OH and C_2H_4(Figure 4c). They compared the C1 and C_2 reaction pathways and found that

CuCr HDACs exhibits the lowest limiting potential of –0.58 V for CO_2RR to C_2 products. Sun et al.[77] used the self-validated machine learning method to investigate the graphdiyne-based dual atom catalyst. They demonstrated that the stability and electroactivity can be optimized by introducing selected lanthanide metals to the transition metals. Additionally, they further verified that the f—d orbital coupling is the pivotal factor in modulating the d-band center, leading to enhanced stability.

2.2. Metal Oxides

Metal oxides are also excellent substrates for supporting well-dispersed metal atoms.[78,79] For instance, Fu et al.[80] investigated the catalytic chemoselectivity of a dual single-atom catalyst $IrMo/TiO_2$ for the hydrogenation of 4-nitrostyrene to 4-vinylaniline and compared it with the corresponding single-atom catalysts Ir/TiO_2 and Mo/TiO_2 (**Figure 5**a). They discovered that the IrMo atom pair is more thermodynamically preferred on TiO_2 substrate than the two Mo or two Ir atom pairs. The 4-nitrostyrene is absorbed on the active site via the nitro group due to the much lower adsorption energies. The Ir atoms are very active to dissociate H_2 molecules, which can provide the H resource for the hydrogenation steps. They calculated the reaction pathway for the key process of the hydrogenation of 4-nitrostyrene (Figure 5b). The H_2 molecule was first dissociated to form Ir—H and H—O—Ti bonds. Then, the H atom was transferred to the absorbed 4-nitrostyrene molecular to hydrogenate the nitro group. The calculation results show that the rate-determining step was the oxygen atom removed from 4-nitrostyrene with the largest energy barrier of 0.80 eV. Remarkably, they concluded that the synergistic cooperation between the two sets of single atoms can greatly improve the catalytic activity and selectivity toward hydrogenation reactions.

2.3. Metal–Organic Frameworks

Metal–organic frameworks (MOFs) are emerging as a new class of candidates in various electrochemical reactions due to their flexible tailorability, ultrahigh surface areas, hollow porous, and well-defined ordered structures.[10,81–83] These features

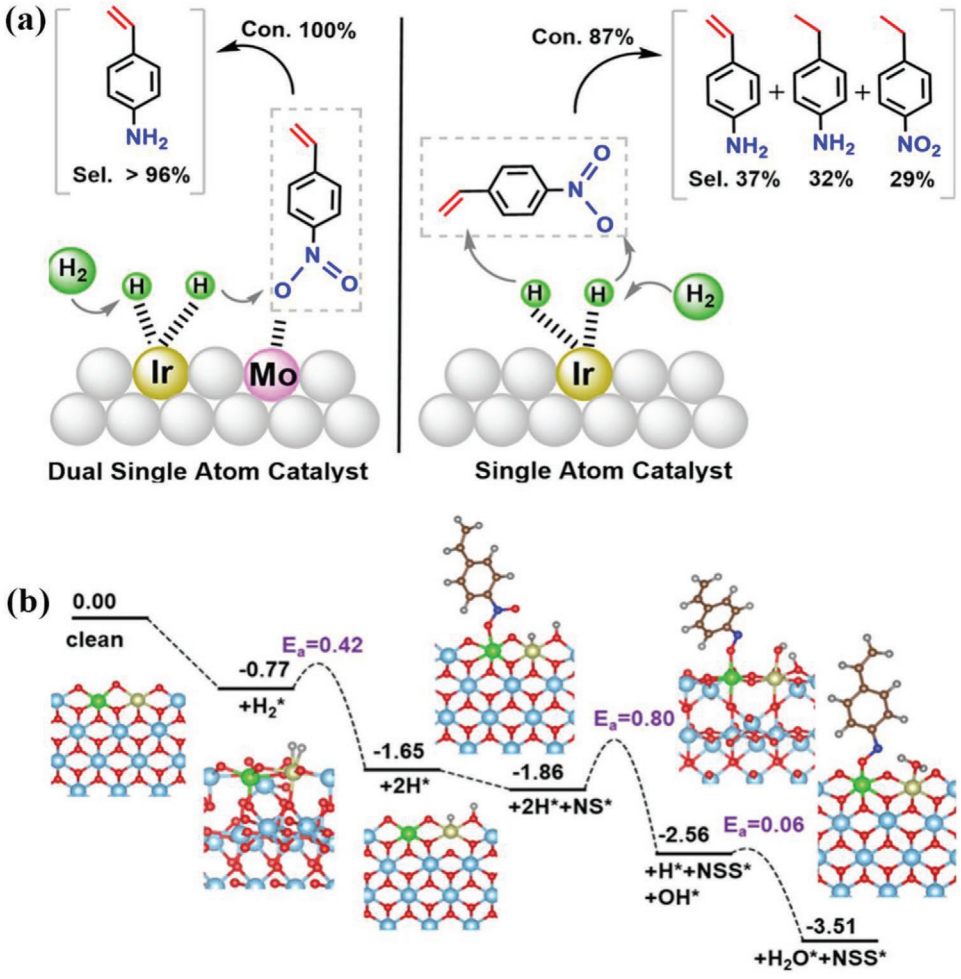

Figure 5. a) The dual single atom and single atom active sites on TiO2 surface for the hydrogenation of 4-nitrostyrene to 4-vinylaniline. b) The energy digram for catalytic deoxygenation of 4-nitrostyrene to4-nitrosostyrene on IrMo/TiO2 catalyst. Reproduced with permission.[80] Copyright 2021, American Chemical Society.

enable MOFs to be ideal supports for designing atomic-level catalysts.[84–86] Moreover, the guest atoms can be confined into the pore spaces in MOFs, which can significantly prevent the migration of metal atoms during the reaction process. Wang et al.[87,88] developed Fe–Co dual sites embedded on N-doped porous carbon and exhibited superior ORR catalytic performance. The heteronuclear dual sites are favored to active O–O bonds, leading to the four-electron oxygen reduction pathway in acidic electrolyte. Cheng et al.[89] investigated the NiMn-based bimetal–organic framework as an efficient OER and ORR catalyst. The calculation results showed that Ni acts as the real active site while Mn serves as the synergetic sites during the oxygen electrocatalysis. The strong synergetic effect between Ni and Mn sites greatly boosts the kinetics of OER and ORR.

3. Experimental Exploration of HDACs

Currently, the so-called single-atom catalysts (SACs) are gaining an increasing interest in the scientific community as unique bridges between homogeneous and heterogeneous catalysis.[90] The last decade has witnessed a myriad of tremendous advances toward the development of SACs for different electrocatalytic reactions such as ORR, NRR, and CO_2RR.[91–93] Despite all these remarkable achievements, SACs exhibit a lack of heteronuclear dual-atom centers that can behave as synergistic active sites, which significantly decrease their possibilities to push the limits of the catalytic rates of many electrocatalytic reactions. Therefore, the introduction of dual catalytic active sites on different substrates has been recently proposed as a promising strategy for a new generation of ultra-efficient atomic catalysts.[42] It is undoubtedly improving our deep understanding of the "synergistic effect" at the atomic level as well as the nature of the interactions between the atomic metal species and the surrounding chemical environment, thus triggering the development of advanced dual atomic catalysts. Specifically, the heteronuclear metal atom catalysis optimizes very important electrocatalytic parameters, such as activity, stability, and selectivity, via tuning the electronic structure of metal active centers, maximizing the atom utilization and improving the overall catalytic performance. Notably, the experimental design of these exciting nanomaterials is still in its infancy due to the inaccurate synthetic approaches and the lack of precision to control the formation of well-dispersed heteronuclear dual-metallic centers as well as the limitations to determine the exact crystallographic structures and active sites.[94] In this regard, those synthetic strategies that can assure both the effective covalent coordination among the metal atoms in the dimeric units and the solid coordination between the metallic dimers and the local environment have been demonstrated to be the way to develop stable double-atom architectures. In this section, we will discuss the most recent experimental advances on the structure–function relationship of experimentally designed dual-atom catalytic systems based on different supports such as low-dimensional materials (0D, 1D, or 2D networks), metal oxides, and MOFs. The plausible mechanisms that govern their catalytic activities toward water splitting reactions, NRR, and CO_2RR and their practical applications for the assembly of energy-related devices such as Zn–air batteries are also illustrated.

3.1. Low Dimensional Networks

Bimetal atom catalysts represent an appealing strategy to greatly boost the electrocatalytic rates of water splitting reactions such as HER, ORR, and OER. Such improvement can be achieved owing to the synergistic interaction of the neighboring atoms into a low-dimensional network, which creates a unique electronic environment at the atomic level, thus facilitating the thermodynamics of the energetic processes of the catalytic species. Yao and coworkers have developed a pioneering methodology to fabricate atomically distributed Pt–Co dimers into nitrogen doped-carbon networks (denoted as A–CoPt–NC) for high-performance ORR electrocatalysis.[95] The as-synthesized A–CoPt–NC materials were built following a two-step synthetic methodology (**Figure 6**a). First, the Co–MOF was carbonized at 850 °C in a nitrogen atmosphere to form the 0D-core-shell Co–NC structure. Second, Pt atoms were electrochemically deposited into the carbon-shell framework by applying a cyclic potential to the Co–NC electrode. The fine structure of the Co and Pt of the as-synthesized dual atomic catalysts was deeply investigated using both X-ray absorption near edge structure (XANES) and X-ray absorption fine structure (EXAFS) spectroscopies (Figure 6a,b). Remarkably, the intensity of the Co–Co peak of the k^2-weighted Fourier transform spectrum of the A–CoPt–NC catalysts experimented a notable decay after the electrochemical activation step (Figure 6b), revealing a change in the inner coordination sphere of Co atoms as well as the dissolution of the metallic Co cores, which was also supported via aberration-corrected STEM and ICP-AES techniques. The high intensity of the white line of A-CoPt-NC in the XANES (inset of Figure 6b) suggests that Co atoms are exhibiting different oxidation states due to the Co–N and/or Co–C and/or Co–C/N coordination environments. The electrochemical performance of the dual atomic catalysts for ORR was evaluated using linear sweep voltammetry in 0.1 M KOH electrolyte at 1600 rpm (Figure 6d). The A–CoPt–NC surpasses the catalytic performance of Co–NC and Pt/C catalysts, exhibiting an impressive half-wave potential of 0.96 V versus RHE, which is 90 mv superior to that of the Pt/C benchmark catalyst. Additionally, the A–CoPt–NC catalyst significantly outperformed the mass activity and specific activity values of Pt/C (Figure 6e), indicating that the dual-atom active sites constitute a more energetically efficient alternative toward ORR electrocatalysis. The impressive catalytic performance of the A–CoPt–NC catalyst was associated with the strong electronic polarization in the Pt–Co atomic pairs, which triggers the electron gathering on the atomic Co cores, thus speeding up the electrocatalytic yields. Consequently, the dual-atom synthetic strategy has shown that the appropriate chemical coordination of Pt atomic species will lead to the effective optimization of their electronic structures for electrocatalysis, ending up with more active and inexpensive Pt-containing catalysts. In this regard, DFT calculations revealed that the remarkable electrocatalytic activity of the Co–Pt dual atomic ORR electrocatalysts is originated by the charge redistribution and the d orbital shift due to the structural arrangement of Pt and Co atoms.

The dual-atom synthetic strategy has also been used to build cost-effective ORR/OER bifunctional catalysts with very prospective properties for the construction of rechargeable zinc–air

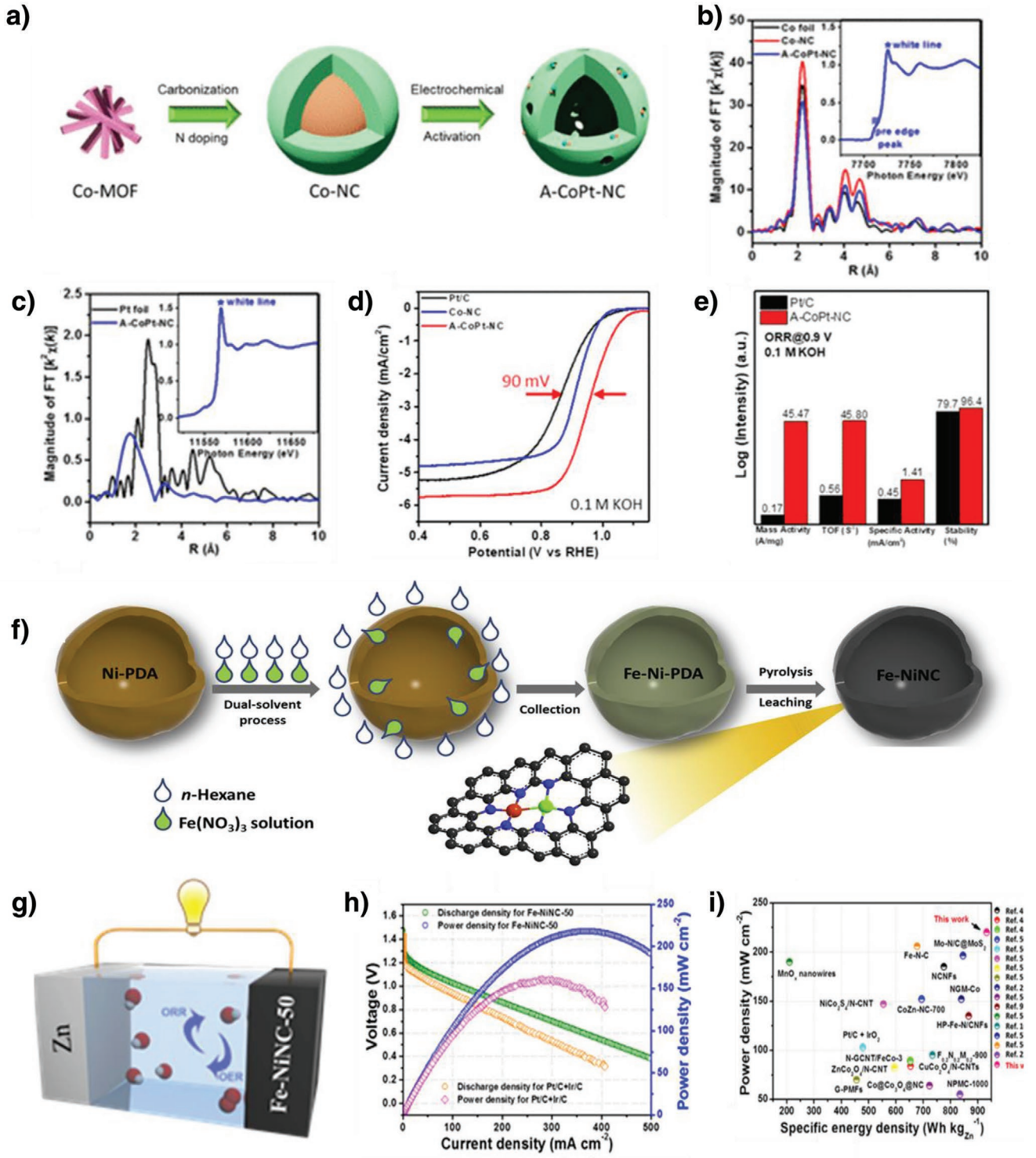

Figure 6. a) Schematic representation of the synthetic approach of the A–CoPt–NC. b,c) The k^2-weight Fourier transform spectra of the Co and Pt EXAFS for Co foil, Pt foil, Co–NC, and A–CoPt–NC, respectively. The insets are the Co and Pt XANES spectra. d) ORR polarization curves of Co–NC, A–CoPt–NC, and Pt/C in 0.1 M KOH at 1600 rpm. e) Comparison of mass activity, specific activity, TOF, and stability of the A–CoPt–NC and Pt/C for ORR. Reproduced with permission.[95] Copyright 2018, American Chemical Society. f) Schematic illustration of the dual-solvent strategy for the Fe–NiNC-50 catalysts. g) Zn–air battery setup. h) Discharge polarization curves and the corresponding power densities for the Fe–NiNC bimetal single catalysts and i) a comparison of the peak power density and specific energy density for the state-of-the-art catalysts. Reproduced with permission.[100] Copyright 2020, Elsevier.

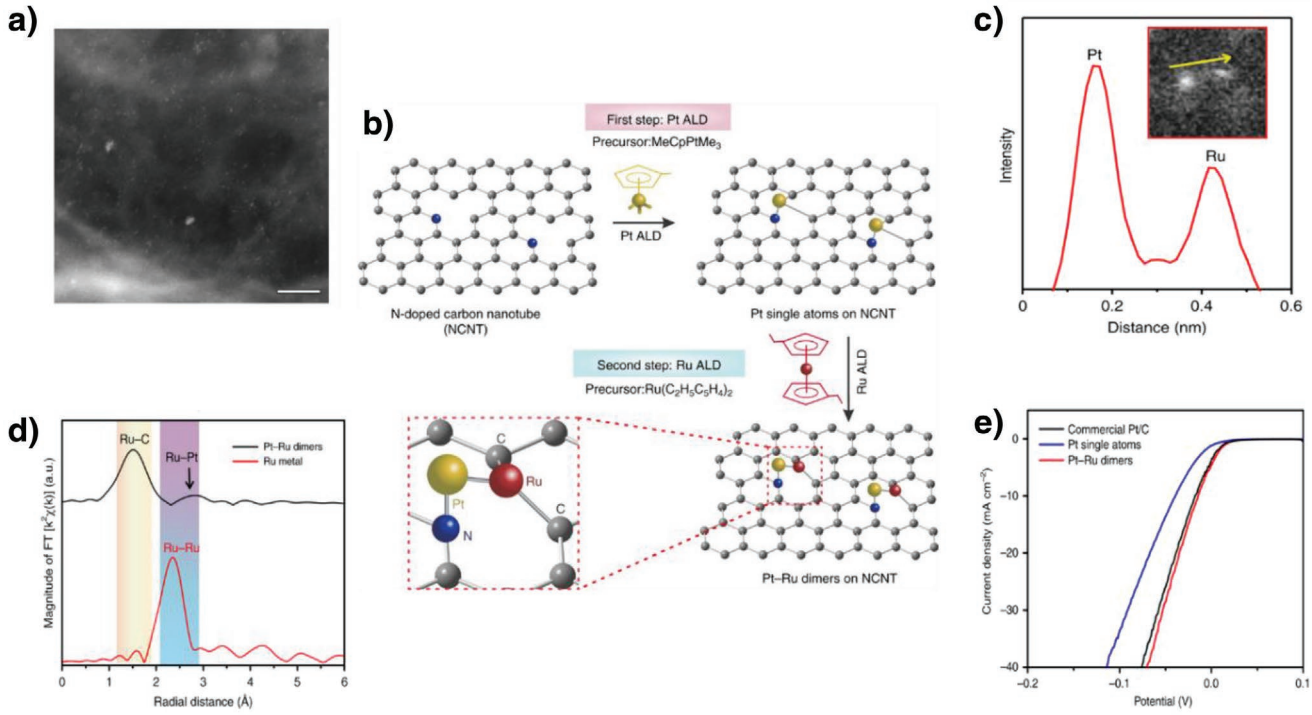

Figure 7. a) Aberration-corrected HAADF–STEM images of Pt–Ru dimers/NCTs. Scale bar 5 nm. b) Scheme of the synthetic strategy to fabricate Pt–Ru dimers on nitrogen-doped carbon nanotubes. c) The intensity profile obtained on one individual Pt–Ru dimer. d) The k2-weight Fourier transform spectra from EXAFS of the Pt foil, Pt SACs, and Pt-Ru dimers. e) Electrocatalytic activity toward HER for the Pt–Ru dimer catalysts. Reproduced with permission.[102] Copyright 2019, Springer Nature.

batteries.[96–99] For instance, Xunju Lu and coworkers reported an N-doped porous carbon-containing atomic Fe–Ni dual-metal pairs that were synthesized by a facile one-pot dual-solvent ion deposition method.[100] The Ni-doped polydopamine (Ni–PDA) was first dispersed in *n*-hexane under sonication (Figure 6f). Afterward, a certain amount of aqueous $Fe(NO_3)_3$ solution was dropwise added into the solution and the final suspension was properly calcinated to form the Fe–NiNC 0D-hollow spheres with the optimized Fe:Ni (1:1) molar ratio (Fe–NiNC-50). The nature of the Ni–Fe bimetal atomic sites was decisively unraveled by using XANES and Fourier-transformed (FT) k^3-weighted extended X-ray absorption fine structure. The Fe–Ni metallic binding was fitted at a position of 2.74–2.89 Å with a coordination number of ≈1 and Fe–N and Ni–N paths were determined to be 3 and 3.3, respectively.

The optimized Fe–NiNC-50 catalysts delivered an excellent bifunctional OER/ORR activity showing a small gap of 0.73 V between the potential of OER to reach 10 $mA \cdot cm^{-2}$ (1.57 V vs RHE) and the half-wave potential of ORR (0.84 V vs RHE). To validate the potential of Fe–NiNC catalysts and substitute the noble-metals as cathodes of zinc–air batteries, a customized Zn–air battery device was constructed employing Fe–NiNC-50 as the cathode (Figure 6g). The device rendered an open circuit of 1.41 V and a remarkable value of power density around 220 $mW \cdot cm^{-2}$ at the corresponding current density of 365 $mA \cdot cm^{-2}$ (Figure 6h). Furthermore, the specific capacity of the Fe–NiNC-50 based ZABs was estimated to be 752.14 $mAh \cdot g^{-1}$, which is associated with a high energy density of ≈923 $Wh \cdot kg_{Zn}^{-1}$, thus surpassing mostly all the ZAB catalysts reported up to now in the literature (Figure 6i).[101] The impressive catalytic yields of the Fe–NiNC-50 catalysts were ascribed to the charge redistribution process in the Fe–Ni bimetal atom moieties, which creates very active catalytic centers for bifunctional OER/ORR electrocatalysis. This work paved the way toward the development of multifunctional dual-atom catalysts by taking advantage of the electron density redistribution in non-precious atomically dispersed biatomic catalytic centers.

Bimetal atom structures have achieved better electrocatalytic rates than that of commercial Pt/C catalysts for hydrogen evolution reactions (HER). Pt–Ru bimetal atom structures were accurately prepared by a two-step atomic layer deposition methodology (**Figure 7**b).[102] First, Pt atoms were atomically deposited onto nitrogen-doped 1D-carbon nanotubes (NCNTs), taking advantage of the well-favorable chemical interaction between Pt SAs and N atoms. Second, the ALD of Ru on Pt single atoms using bis(ethylcyclopentadienyl)ruthenium (II) was performed to obtain the Pt–Ru atomic dimers. The atomic resolution of the HAAD–STEM images confirmed the dimer-like structure of the as-synthesized electrocatalysts (Figure 7a). Accordingly, the two atoms showed different contrast, indicating their different metallic character (Figure 7c). In addition, the Pt–Ru dimer nature was also demonstrated by X-ray absorption spectroscopy (XAS) results (Figure 7d). The Pt–Ru dimers displayed a clear Ru–C peak at ≈1.6 Å and a relatively weak peak at ≈2.8 Å. The peak at 1. 6 Å can be assigned to Ru−C chemical bonds. The small peak at 2.8 Å is ascribed to the Pt−Ru scattering. It is worth noting that the k dependence of the backscattering amplitude of these bigger atoms oscillates in the k space, thus giving

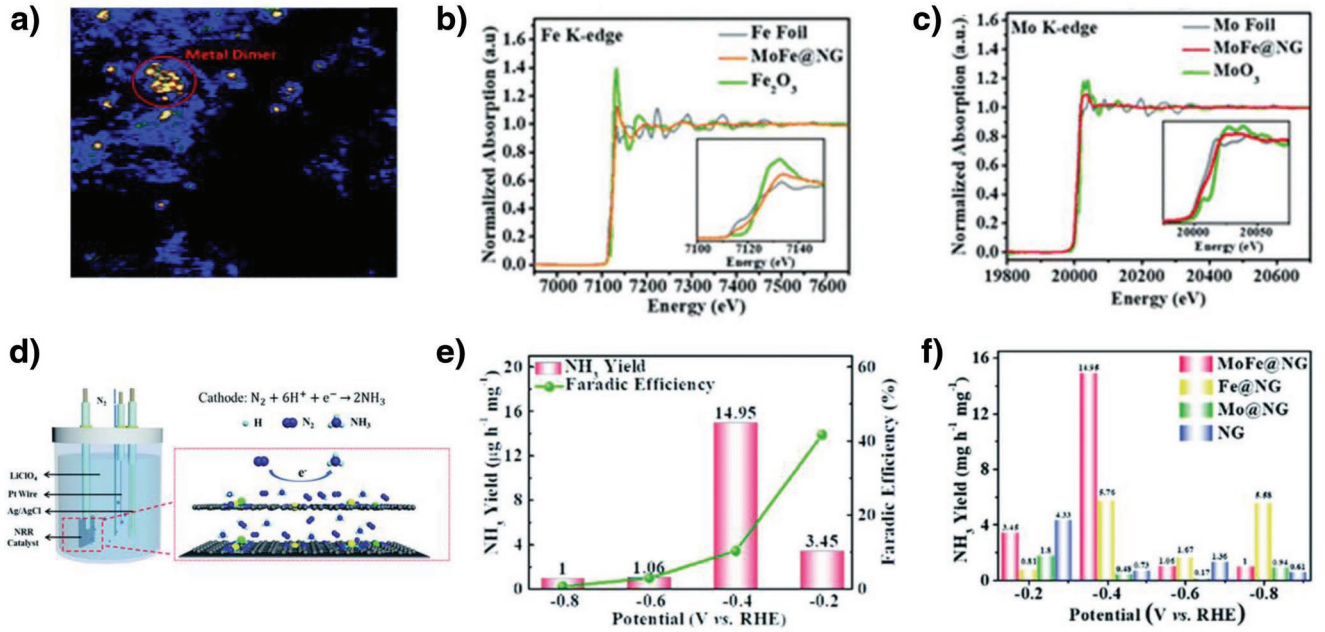

Figure 8. a) The HAADF–STEM images of FeMo@NG catalysts. b,c) Normalized XANES spectra at the Mo K-edge and the Fe K-edge for MoFe@NG, respectively. The insets show an enlarged view of metal K-edge section of the XANES spectra. d) Schematic representation of the NRR reactor. e) NH_3 yields and faradaic efficiencies for MoFe@NG at different potentials. f) NH_3 yield rates of NG, Fe@NG, Mo@NG, and MoFe@NG at different electrochemical potentials. Reproduced with permission.[103] Copyright 2019, Royal Society of Chemistry.

rise to a non-symmetric FT peak. The electrocatalytic activity of the Pt—Ru dual atom catalysts, Pt SAs, and commercial Pt/C toward HER were assessed by linear sweep voltammetry in 0.5 M H_2SO_4 (Figure 7e). The mass HER activities of all catalysts were calculated based on the mass loading at 0.05 V versus RHE. Remarkably, the Pt—Ru bimetal atom catalysts show a mass activity of 23.1 $A \cdot mg^{-1}$, which is 54 times larger than that of commercial Pt/C, thus demonstrating the superior HER intrinsic catalytic activity of the dimers. It was linked to the synergistic effect of the Pt—Ru dimer on their electronic density states, which significantly increased the HER rates. This work opened new horizons toward the precise manipulation of dual-metal dimers for superior HER electrocatalysis.

Dual atoms catalysts have been recently employed to selectively speed up the nitrogen reduction reaction (NRR) kinetics. N-doped 2D-graphene successfully behaved as a suitable platform to integrate Mo and Fe atoms with equal molar ratios into metal dimer species at the atomic level.[103] The newly synthesized dual-atom catalysts (denoted as FeMo@NG) were fabricated via a typical template-based synthetic strategy and the resulting dimer structure was fully verified using HAAD–STEM and XANES spectra at both Fe–K edge and Mo–K edge (**Figure 8**a,b,c). The electrocatalytic NRR performance of MoFe@NG was performed by chronoamperometry in N_2-saturated electrolyte for 6 h in a 3-electrode electrolytic cell (Figure 8d). As shown in Figure 8e, the dual-atom MoFe@NG catalysts achieved the highest NH_3 yield rate of 14.95 mg h^{-1} mg^{-1} at –0.4 V, while the larger FE of 41% was obtained at –0.2 V. Additionally, MoFe@NG showed better NH_3 yields than those of the monoatomic systems at lower electrochemical potentials, suggesting its superior NRR electrochemical performance (Figure 8f). The nature-inspired $FeMoN_6$ active sites of the MoFe@NG structures facilitate both the weakening of the N≡N bonds and a more energetically favorable alternative NRR mechanistic pathway, placing it as the first application of bioinspired bimetal atomic configurations for superior NRR electrocatalysis.

3.2. Metal Oxides

Porphyrin-derived non-precious bimetallic single atoms nanomaterials using silica nanoparticles as effective templates constitute an excellent alternative to develop durable catalysts for ORR and, in turn, highly functional zinc–air batteries. In this regard, atomically dispersed bimetallic Fe/Co catalytic active sites within N-doped carbon networks (Fe/Co–N_x–C) have been successfully synthesized via pyrolysis of metal-coordinated polyporphyrin structures (**Figure 9**a).[104] To maximize the specific surface area, the electron conductivity and therefore the ORR electrocatalytic performance of the resulting electrocatalysts, three synthetic strategies were applied. 1) A porphyrin network functionalized with Fe and Co species was used as a precursor to fabricate the dual-atom Fe/Co sites on N-doped carbon frameworks. 2) Silica nanoparticles were utilized as templates to improve the number of mesopores in the catalyst structure. 3) The silica protection fulfills a dual function during the synthesis by protecting the integration of the metal-functionalized porphyrin framework and boosting the number of accessible sites.

Notably, the aberration-corrected HAADF–STEM reveals a myriad of isolated bright spots with diameters of ≈0.1–0.2 nm (Figure 9b), demonstrating the presence of isolated Fe and Co atoms, which are anchored to the carbon network. The

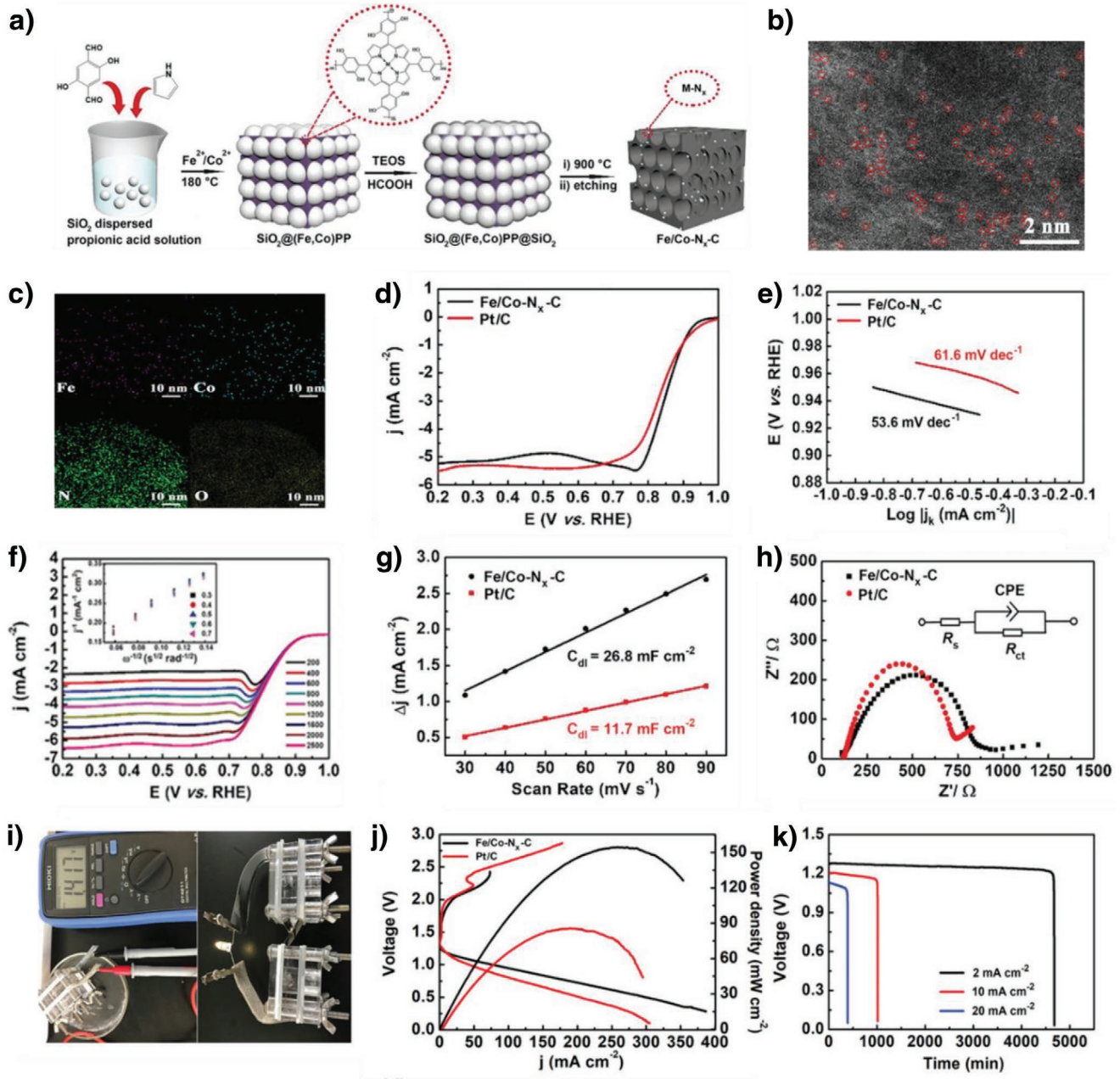

Figure 9. a) Synthetic procedure to fabricate the Fe/Co–N_x–C catalysts. b) Aberration-corrected HAADF–STEM image and c) EDS elemental mapping images of Fe/Co–N_x–C. d) ORR LSV curves and e) their corresponding Tafel plots of Fe/Co–N_x–C and Pt/C in O_2-saturated KOH solution at 1600 rpm. f) LSVs curves for ORR at different rotation speeds and the corresponding *K*–*L* plots for the Fe/Co–N_x–C catalysts. g) The values of C_{dl} for Fe/Co–N_x–C and Pt/C. h) Nyquist plots for Fe/Co–N_x–C and Pt/C catalysts. i) Photograph of the ZAB system measured at open-circuit voltage and the corresponding LED arrangement. j) LSV and power density curves of the ZABs containing Fe/Co–N_x–C and Pt/C as the air cathode nanomaterials. k) Long-term galvanostatic discharge curves of ZABs with Fe/Co–N_x–C as cathode catalysts. Reproduced with permission.[104] Copyright 2020, Wiley.

EDS-based elemental mapping of Fe/Co–N_x–C catalysts further confirmed that the Fe, Co, C, N, and O elements are homogeneously dispersed within the bimetal atom matrix (Figure 9c). Impressively, the Fe/Co–N_x–C catalysts rendered a very competitive value of the half-wave potential of 0.86 V versus RHE and an ultralow Tafel slope (53.6 mV·dec^{-1}), thus improving the values reached by Pt/C benchmark catalysts (0.84 V vs RHE and 61.6 mV·dec^{-1}) (Figure 9d,e). The kinetics ORR properties of the Fe/Co–N_x–C bimetal atom networks were also studied using an RDE spinning at different rotational speeds (Figure 9f). The corresponding Koutechy–Levich (L–K) shows a linear relationship between the reciprocal current density (j^{-1}) and the negative square root of rotating speed ($\omega^{-1/2}$) in a very wide potential window, thus implying the ORR rates are following a first-order reaction in the Fe/Co–N_x–C.[105] The average electron transfer number was estimated to be 3.81,

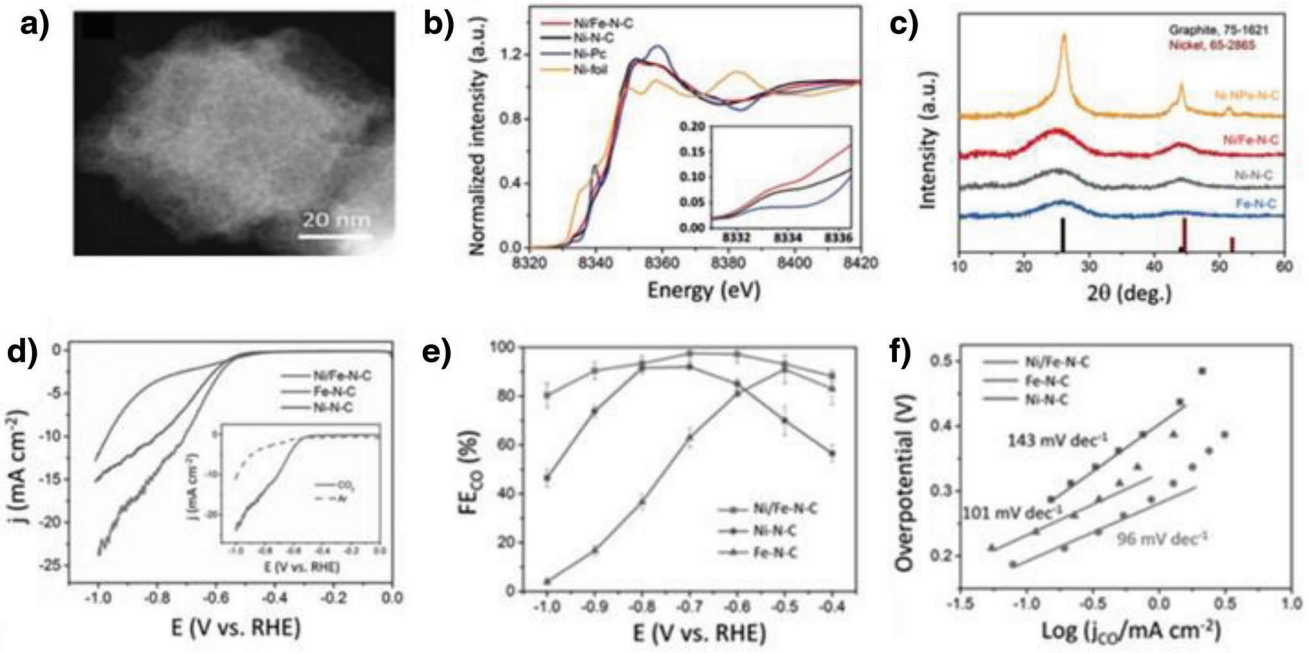

Figure 10. a) Aberration-corrected HAAD–STEM image of the Ni/Fe–N–C. b) XRD patterns and c) Ni-edge XANES spectra for Ni foil, Ni–N–C, Fe–N–C, and Ni/Fe–M–C catalysts. d) LSVs for the as-synthesized catalysts in CO_2-saturated 0.5 M $KHCO_3$ catalysts. e) FE_{CO} and f) TOF values of the catalysts. Reproduced with permission.[106] Copyright 2019, Wiley.

which reveals that the catalytic reaction follows a highly effective four-electron reduction pathway. It is worth noting that the bimetal single catalyst exhibited improved double-layer capacitance (C_{DL}) and charge transfer resistant (R_{CT}) values compared with those of Pt/C (Figure 9g,h), which reflects both the higher number of catalytically active sites and remarkable electrokinetic efficiency of the non-precious dual-atom N-doped carbon networks. Also, the Fe/Co–N_x–C nanomaterials showed an outstanding electrochemical behavior as an air cathode for aqueous ZABs (Figure 9i,j) and Figure 9k). They displayed a peak power density of 152 mW·cm^{-2}, thus beating the Pt/C-based ZAB cathodes (87 mW·cm^{-2}) (Figure 9j). Additionally, the porphyrin-derived bimetal atom catalysts showed superior durability properties, giving off a stable voltage output of 1.27 V at the discharge current density of 2 mA cm^{-2} for 77 h (Figure 9k).

3.3. Metallic–Organic Frameworks

Recently, metal–organic frameworks (MOFs) have demonstrated a unique strategy for fabricating single/dual-atom and cluster catalysts, featuring the distinctive advantages of high metal loadings, porous structures, and tailorable catalytic sites.[10] Catalysts consisting of atomically dispersed transition metals attached to N-doped carbon networks have also yielded impressive rates for CO_2 electroreduction. Particularly, diatomic Ni–Fe metal-nitrogen sites (Ni/Fe–N–C) have exhibited huge efficiencies for CO_2RR.[106] The isolated diatomic Ni–Fe metal–nitrogen catalyst was synthesized following an ion-exchange strategy based on the pyrolysis of a Zn/Ni/Fe zeolitic imidazolate framework. The Ni–Fe dimer-like structure was fully verified by HAAD–STEM, Ni K-edge XANES spectra, and XRD techniques (**Figure 10**a,b,c). The electrocatalytic activity of Fe–N–C, Ni–N–C, and Ni/Fe–N–C for CO_2RR was performed using a three-electrode H-cell with CO_2-saturated 0.5 M $KHCO_3$ solution as the electrolyte (Figure 10d). As is shown in the LSV trend, Ni/Fe–N–C rendered the highest total current density from –0.6 to –1.0 V (vs RHE), reaching current densities of 9.5 mA·cm^{-2} at –0.7 V and 23.7 mA cm^{-2} at –1.0 V (vs RHE), thus surpassing those of the Fe and Ni SACs. Besides, Ni/Fe–N–C catalysts exceed the Faradaic efficiency (FE) values of CO generated across the entire potential window from –0.4 to –1.0 V, achieving an optimal FE value of 98% at –0.7 V (Figure 10e). It was also supported by the lowest Tafel slope (96 mV·s^{-1}) of the Ni/Fe–N–C catalyst (Figure 10f), which implies an extra improvement on the kinetic of the first electron transfer step of the bimetal atoms. Notably, the superior catalytic rates of Ni/Fe–N–C catalysts were explained based on the synergetic interatomic interaction of the Ni–Fe dimers, which not only triggers the lowering of the energetic barriers for the formation of COOH* and the desorption of CO, but also induces energetically favorable structural changes into the CO-adsorbed catalytic species.

Remarkably, Jing Wang and coworkers have discovered an attractive host–guest strategy to build Fe–Co dual atom catalytic centers for acidic ORR electrocatalysis using bimetallic MOF as host architectures.[87] Particularly, a Zn/Co bimetallic MOF, comprising Co^{2+} and Zn^{2+} nodes, was used as a host to encapsulate $FeCl_3$ molecules within cavities. The resulting supramolecular structure was pyrolyzed to the desired temperature (1173 K) for 2 h under flowing Ar gas and then naturally cooled down to obtain the (Fe,Co)/N–C electrocatalysts (**Figure 11**a). The as-synthesized catalysts showed better catalytic performances

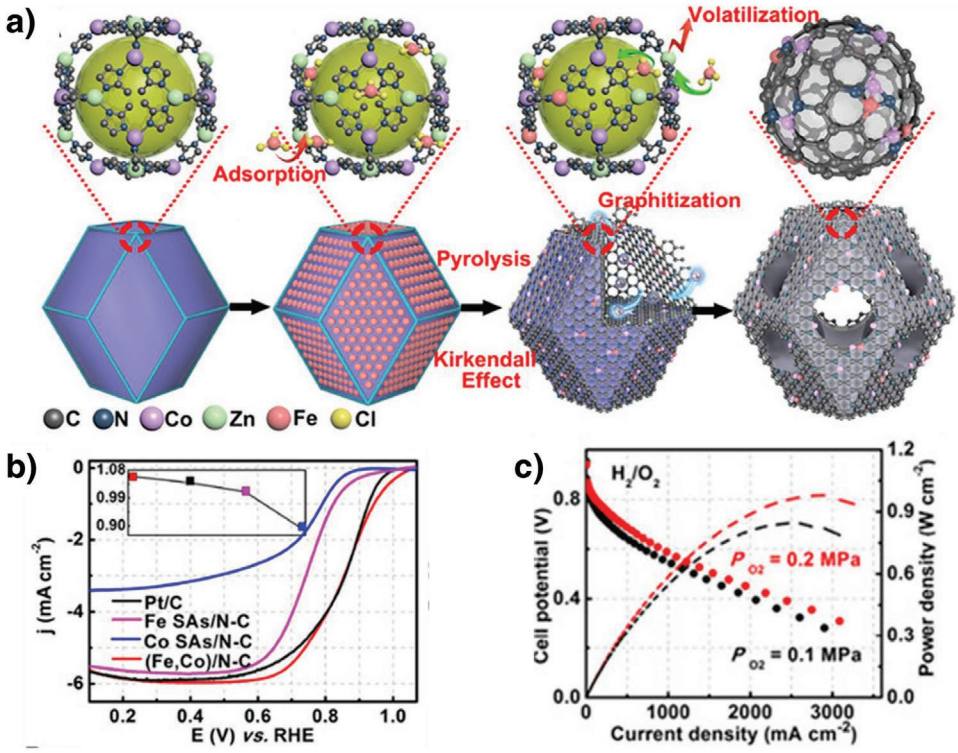

Figure 11. a) Synthetic approach of the (Fe,Co)N–C. b) RDE polarization curves of Pt/C, Co SAs/N–C, Fe SAs/N–C, and (Fe,Co)/N–C in O2-saturated 0.1 M HClO4 solutions at 1600 rpm. Inset: E_{onset} of different catalysts. c) H_2/O_2 fuel cell polarization plots. Cathode: ≈ 0.77 mg cm^{-2} of (Fe,Co)/N–C; 100% RH; O_2, and 0.1 and 0.2 MPa partial pressures. Anode: 0.1 mg_{Pt} cm^{-2} Pt/C; 100%. Reproduced with permission.[87] Copyright 2017, American Chemical Society.

compared with those of Fe SAs/N–C, Co SAs/N–C, and commercial Pt/C catalysts (Figure 11b), delivering a superior ORR electrocatalytic activity at acidic environments, which is characterized by a half-wave potential of 0.86 V versus RHE and an onset potential of 1.06 V versus RHE and also exceeded the catalytic activity of most of the non-precious catalysts reported up to now. The (Fe,Co)/N–C catalysts were tested as a cathode of a H_2/O_2 fuel cell device. Using O_2 as oxidant, the (Fe,Co)/N-C dual atomic catalysts rendered a maximum power density value of ≈0.85 and 0.98 W cm^{-2}, respectively, thus decreasing the gap between the non-precious and Pt/C catalysts. This cathodic electrode with dual metal sites behaves as an ultra-stable electrode in a long-term operation with 50 000 cycles for electrode measurement and 100 h for H2/air single cell device. For the first time, atomic catalyst architectures can deliver a Pt-like activity towards acidic ORR electrocatalytic reactions.

4. Conclusion and Outlook

Although heteronuclear dual-atom catalysts have demonstrated very powerful physical–chemistry properties for a large battery of electrocatalytic reactions, the correlation between the structural and/or conformational changes of the atomically dispersed bimetallic centers and the mechanistic pathways of the catalytic reactions have remained largely unsolved, which need the combination of both new theory and experimental insights. First, the stability of the HDACs is the primary problem of these kinds of catalysts. Compared with the single atomic sites in SACs, heteronuclear dual-atom sites are more difficult to be precisely controlled, especially under real reaction conditions. Second, the current substrates for anchoring the heteronuclear dual-atom are mostly limited to 2D materials. The development of more suitable substrates to effectively anchor atoms is of paramount significance.[107] Moreover, the deep investigation of the interaction between the substrate and supported atoms is of crucial importance to search for efficient strategies to enhance the stability of HDACs. Second, the correlation between the activity and the structure catalytic performance of HDACs should be further explored. For instance, it is still unclear for HDACs if both atoms are active in the reaction mechanism. To uncover the underlying reasons why this asymmetric active site could enhance the catalytic behavior compared to the symmetric center is of significant importance. Thus, a better understanding of the relationship of "structure–performance" and taking advantage of this asymmetric active center could enable us to design more efficient catalysts. Moreover, the asymmetry-breaking dual active sites that can overcome the traditional linear scaling relation could be used for the rational design of novel catalysts for specific reactions. In addition, the development of machine learning algorithms to quickly predict high-performance candidates could be a powerful tool to accelerate the trial-and-error processes, thus favoring the synthesis of very efficient HDAC electrocatalysts.

From an experimental perspective, the current techniques used for the structural characterization of SACs, including

XAFS, HAADF–STEM, and IR spectroscopy, are not sufficient to accurately disentangle the coordination sphere of both metallic centers of the dual-atom catalysts. Thus, the exploration of the catalytic active sites using in situ measurements, such as in situ XAS and in situ Raman spectroscopy, represents a crucial step to obtain insightful advances toward the deep understanding of the electronic structure–catalytic property relationship of dual-atom catalysts at the sub-nanometer level. It will further pave the way toward the study of the structural variations of the metallic coordination environments during the catalytic reaction and their direct implications on the overall electrocatalytic activity. Most importantly, up to now, mostly all the reported works fail to obtain 100% pure dual-atom structures. Indeed, most of the works reported in the literature cannot fully guarantee that they don't have any single atom contribution in the whole network. We believe that the use of scanning electrochemical microscopy (SECM) to evaluate the electrocatalytic activity of the HDACs will open a new chapter on exploring the catalytic phenomenon at the atomic and/or nanometer level. Additionally, the opportunity to evaluate the electrocatalytic performances of dual atom catalysts at 100 nm^2 spots will facilitate the disentangling of the real electrocatalytic response of these bimetallic centers, thus crucially improving our understanding of their electrocatalytic behavior.

As a rising star in atomic catalysts, HDACs have broad and promising applications in many areas. However, the current study of HDACs is very scarce and mainly limited to water-splitting and oxygen reduction reactions. Briefly, the potential applications of HDACs in NRR, CO2RR, selective hydrogenation reactions, batteries, and other energy-related fields require further theoretical and experimental investigations.

Acknowledgements

T.H. and A.R.P.S. contributed equally to this work. H.P. is thankful for the support of the Science and Technology Development Fund from Macau SAR (FDCT-0102/2019/ A2, FDCT-0035/2019/AGJ, FDCT-0154/2019/A3, FDCT-0033/ 2019/AMJ) from the University of Macau. A. D. greatly appreciates the financial support from the Australian Research Council under Discovery Project (DP170103598).

Open access funding enabled and organized by Projekt DEAL.

Conflict of Interest

The authors declare no conflict of interest.

Keywords

asymmetry active centers, atomic catalysis, heteronuclear dual-atoms, synergistic interactions

Received: October 7, 2021
Revised: November 11, 2021
Published online: December 12, 2021

[1] K. Caldeira, M. E. Wickett, *Nature* **2003**, *425*, 365.
[2] S. Chu, A. Majumdar, *Nature* **2012**, *488*, 294.
[3] B. Dudley, *Report–BP Energy Economics–London: UK* **2019**, 9.
[4] V. R. Stamenkovic, D. Strmcnik, P. P. Lopes, N. M. Markovic, *Nat. Mater.* **2017**, *16*, 57.
[5] Z. W. Seh, J. Kibsgaard, C. F. Dickens, I. Chorkendorff, J. K. Nørskov, T. F. Jaramillo, *Science* **2017**, *355*, 355..
[6] K. Yamamoto, T. Imaoka, W.-J. Chun, O. Enoki, H. Katoh, M. Takenaga, A. Sonoi, *Nat. Chem.* **2009**, *1*, 397.
[7] L. Liu, A. Corma, *Chem. Rev.* **2018**, *118*, 4981.
[8] Y. Chen, S. Ji, C. Chen, Q. Peng, D. Wang, Y. Li, *Joule* **2018**, *2*, 1242.
[9] L. Jiao, H.-L. Jiang, *Chem* **2019**, *5*, 786.
[10] C.-C. Hou, H.-F. Wang, C. Li, Q. Xu, *Energy Environ. Sci.* **2020**, *13*, 1658.
[11] J. Fu, J. Lym, W. Zheng, K. Alexopoulos, A. V. Mironenko, N. Li, J. A. Boscoboinik, D. Su, R. T. Weber, D. G. Vlachos, *Nat. Catal.* **2020**, *3*, 446.
[12] M. Liu, Z. Zhao, X. Duan, Y. Huang, *Adv. Mater.* **2019**, *31*, 1802234.
[13] R. Lin, X. Cai, H. Zeng, Z. Yu, *Adv. Mater.* **2018**, *30*, 1705332.
[14] J. Zhang, L. Wang, B. Zhang, H. Zhao, U. Kolb, Y. Zhu, L. Liu, Y. Han, G. Wang, C. Wang, *Nat. Catal.* **2018**, *1*, 540.
[15] Z. Li, Q. Xu, *Acc. Chem. Res.* **2017**, *50*, 1449.
[16] J. Mao, W. Chen, D. He, J. Wan, J. Pei, J. Dong, Y. Wang, P. An, Z. Jin, W. Xing, *Sci. Adv.* **2017**, *3*, e1603068.
[17] S. Tian, Q. Fu, W. Chen, Q. Feng, Z. Chen, J. Zhang, W.-C. Cheong, R. Yu, L. Gu, J. Dong, *Nat. Commun.* **2018**, *9*, 1.
[18] C. Xie, Z. Niu, D. Kim, M. Li, P. Yang, *Chem. Rev.* **2019**, *120*, 1184.
[19] H. Fei, J. Dong, D. Chen, T. Hu, X. Duan, I. Shakir, Y. Huang, X. Duan, *Chem. Soc. Rev.* **2019**, *48*, 5207.
[20] L. Wang, W. Chen, D. Zhang, Y. Du, R. Amal, S. Qiao, J. Wu, Z. Yin, *Chem. Soc. Rev.* **2019**, *48*, 5310.
[21] T. He, L. Zhang, G. Kour, A. Du, *J. CO2 Util.* **2020**, *37*, 272.
[22] B. Qiao, A. Wang, X. Yang, L. F. Allard, Z. Jiang, Y. Cui, J. Liu, J. Li, T. Zhang, *Nat. Chem.* **2011**, *3*, 634.
[23] J. Han, J. Bian, C. Sun, *Research* **2020**, *2020*, 9512763.
[24] T. He, C. Zhang, L. Zhang, A. Du, *Nano Res.* **2019**, *12*, 1817.
[25] T. He, C. Zhang, A. Du, *Chem. Eng. Sci.* **2019**, *194*, 58.
[26] T. He, S. K. Matta, G. Will, A. Du, *Small Methods* **2019**, *3*, 1800419.
[27] S. Ji, Y. Chen, X. Wang, Z. Zhang, D. Wang, Y. Li, *Chem. Rev.* **2020**, *120*, 11900.
[28] C. Tang, Y. Jiao, B. Shi, J. N. Liu, Z. Xie, X. Chen, Q. Zhang, S. Z. Qiao, *Angew. Chem., Int. Ed.* **2020**, *59*, 9171.
[29] X. Liu, Y. Jiao, Y. Zheng, M. Jaroniec, S.-Z. Qiao, *J. Am. Chem. Soc.* **2019**, *141*, 9664.
[30] T. He, S. K. Matta, A. Du, *Phys. Chem. Chem. Phys.* **2019**, *21*, 1546.
[31] H. Jeong, S. Shin, H. Lee, *ACS Nano* **2020**, *14*, 14355.
[32] J. Liu, D. Cao, H. Xu, D. Cheng, *Nano Select* **2021**, *2*, 251.
[33] J. Jiao, R. Lin, S. Liu, W.-C. Cheong, C. Zhang, Z. Chen, Y. Pan, J. Tang, K. Wu, S.-F. Hung, *Nat. Chem.* **2019**, *11*, 222.
[34] G. Sun, Z.-J. Zhao, R. Mu, S. Zha, L. Li, S. Chen, K. Zang, J. Luo, Z. Li, S. C. Purdy, *Nat. Commun.* **2018**, *9*, 1.
[35] H. Xiao, W. A. Goddard, T. Cheng, Y. Liu, *Proc. Natl. Acad. Sci. USA* **2017**, *114*, E7045.
[36] T. He, G. Kour, X. Mao, A. Du, *J. Catal.* **2020**, *382*, 49.
[37] D. Zhao, Z. Zhuang, X. Cao, C. Zhang, Q. Peng, C. Chen, Y. Li, *Chem. Soc. Rev.* **2020**, *49*, 2215.
[38] S. Chen, M. Cui, Z. Yin, J. Xiong, L. Mi, Y. Li, *ChemSusChem* **2021**, *14*, 73.
[39] Y. Zhou, E. Song, W. Chen, C. U. Segre, J. Zhou, Y. C. Lin, C. Zhu, R. Ma, P. Liu, S. Chu, *Adv. Mater.* **2020**, *32*, 2003484.
[40] C. Wang, K. Wang, Y. Feng, C. Li, X. Zhou, L. Gan, Y. Feng, H. Zhou, B. Zhang, X. Qu, *Adv. Mater.* **2021**, *33*, 2003327.
[41] Y. Pan, C. Zhang, Z. Liu, C. Chen, Y. Li, *Matter* **2020**, *2*, 78.
[42] Y. Ying, X. Luo, J. Qiao, H. Huang, *Adv. Funct. Mater.* **2021**, *31*, 2007423.
[43] Z. He, K. He, A. W. Robertson, A. I. Kirkland, D. Kim, J. Ihm, E. Yoon, G.-D. Lee, J. H. Warner, *Nano Lett.* **2014**, *14*, 3766.

[44] H. Yan, Y. Lin, H. Wu, W. Zhang, Z. Sun, H. Cheng, W. Liu, C. Wang, J. Li, X. Huang, *Nat. Commun.* **2017**, *8*, 1.
[45] M. Xiao, H. Zhang, Y. Chen, J. Zhu, L. Gao, Z. Jin, J. Ge, Z. Jiang, S. Chen, C. Liu, *Nano Energy* **2018**, *46*, 396.
[46] H. Li, L. Wang, Y. Dai, Z. Pu, Z. Lao, Y. Chen, M. Wang, X. Zheng, J. Zhu, W. Zhang, *Nat. Nanotechnol.* **2018**, *13*, 411.
[47] M. Gong, Z. Deng, D. Xiao, L. Han, T. Zhao, Y. Lu, T. Shen, X. Liu, R. Lin, T. Huang, *ACS Catal.* **2019**, *9*, 4488.
[48] G. Hu, L. Shang, T. Sheng, Y. Chen, L. Wang, *Adv. Funct. Mater.* **2020**, *30*, 2002281.
[49] R. T. Hannagan, G. Giannakakis, M. Flytzani-Stephanopoulos, E. C. H. Sykes, *Chem. Rev.* **2020**, *120*, 12044.
[50] W. Ren, X. Tan, J. Qu, S. Li, J. Li, X. Liu, S. P. Ringer, J. M. Cairney, K. Wang, S. C. Smith, *Nat. Commun.* **2021**, *12*, 1.
[51] A. Chen, X. Yu, Y. Zhou, S. Miao, Y. Li, S. Kuld, J. Sehested, J. Liu, T. Aoki, S. Hong, *Nat. Catal.* **2019**, *2*, 334.
[52] S. Back, Y. Jung, *ACS Energy Lett.* **2017**, *2*, 969.
[53] P. Sajith, Y. Shiota, K. Yoshizawa, *ACS Catal.* **2014**, *4*, 2075.
[54] Y. Kong, D. Liu, H. Ai, K. H. Lo, S. Wang, H. Pan, *ACS Appl. Nano Mater.* **2020**, *3*, 11274.
[55] X. Liu, Y. Jiao, Y. Zheng, K. Davey, S.-Z. Qiao, *J. Mater. Chem. A* **2019**, *7*, 3648.
[56] F. Wang, W. Xie, L. Yang, D. Xie, S. Lin, *J. Catal.* **2021**, *396*, 215.
[57] M. A. Hunter, J. M. Fischer, Q. Yuan, M. Hankel, D. J. Searles, *ACS Catal.* **2019**, *9*, 7660.
[58] X. Zhao, X. Liu, B. Huang, P. Wang, Y. Pei, *J. Mater. Chem. A* **2019**, *7*, 24583.
[59] J. Xu, A. Elangovan, J. Li, B. Liu, *J. Phys. Chem. C* **2021**, *125*, 2334.
[60] R. Hu, Y. Li, Q. Zeng, J. Shang, *Appl. Surf. Sci.* **2020**, *525*, 146588.
[61] Y. Li, R. Hu, Z. Chen, X. Wan, J.-X. Shang, F.-H. Wang, J. Shui, *Nano Res.* **2021**, *14*, 611.
[62] L. Cao, Y. Shao, H. Pan, Z. Lu, *J. Phys. Chem. C* **2020**, *124*, 11301.
[63] C. J. Van der Ham, M. T. Koper, D. G. Hetterscheid, *Chem. Soc. Rev.* **2014**, *43*, 5183.
[64] T. He, A. R. P. Santiago, A. Du, *J. Catal.* **2020**, *388*, 77.
[65] S. Wang, L. Shi, X. Bai, Q. Li, C. Ling, J. Wang, *ACS Cent. Sci.* **2020**, *6*, 1762.
[66] X. Guo, J. Gu, S. Lin, S. Zhang, Z. Chen, S. Huang, *J. Am. Chem. Soc.* **2020**, *142*, 5709.
[67] X. Lv, W. Wei, B. Huang, Y. Dai, T. Frauenheim, *Nano Lett.* **2021**, *21*, 1871.
[68] M. Qu, G. Qin, J. Fan, A. Du, Q. Sun, *Appl. Surf. Sci.* **2021**, *537*, 148012.
[69] Y. Qian, Y. Liu, Y. Zhao, X. Zhang, G. Yu, *EcoMat* **2020**, *2*, e12014.
[70] L. J. Arachchige, Y. Xu, Z. Dai, X. L. Zhang, F. Wang, C. Sun, *J. Mater. Sci. Technol.* **2021**, *77*, 244.
[71] G. Zheng, L. Li, S. Hao, X. Zhang, Z. Tian, L. Chen, *Adv. Theory Simul.* **2020**, *3*, 2000190.
[72] Y. Ouyang, L. Shi, X. Bai, Q. Li, J. Wang, *Chem. Sci.* **2020**, *11*, 1807.
[73] T. He, K. Reuter, A. Du, *J. Mater. Chem. A* **2020**, *8*, 599.
[74] T. He, C. Tang, A. R. P. Santiago, R. Luque, H. Pan, A. Du, *J. Mater. Chem. A* **2021**, *9*, 13192.
[75] L. Li, H. Guo, G. Yao, C. Hu, C. Liu, Z. Tian, B. Li, Q. Zhang, L. Chen, *J. Mater. Chem. A* **2020**, *8*, 22327.
[76] D. Chen, Z. Chen, Z. Lu, J. Tang, X. Zhang, C. V. Singh, *J. Mater. Chem. A* **2020**, *8*, 21241.
[77] M. Sun, T. Wu, A. W. Dougherty, M. Lam, B. Huang, Y. Li, C. H. Yan, *Adv. Energy Mater.* **2021**, *11*, 2003796.
[78] J. Jones, H. Xiong, A. T. DeLaRiva, E. J. Peterson, H. Pham, S. R. Challa, G. Qi, S. Oh, M. H. Wiebenga, X. I. P. Hernández, *Science* **2016**, *353*, 150.
[79] N. J. O'Connor, A. Jonayat, M. J. Janik, T. P. Senftle, *Nat. Catal.* **2018**, *1*, 531.
[80] J. Fu, J. Dong, R. Si, K. Sun, J. Zhang, M. Li, N. Yu, B. Zhang, M. G. Humphrey, Q. Fu, *ACS Catal.* **2021**, *11*, 1952.
[81] H. Furukawa, K. Cordova, *Science* **2013**, *341*, 1230444.
[82] M. Higuchi, D. Tanaka, S. Horike, H. Sakamoto, K. Nakamura, Y. Takashima, Y. Hijikata, N. Yanai, J. Kim, K. Kato, *J. Am. Chem. Soc.* **2009**, *131*, 10336.
[83] A. J. Howarth, Y. Liu, P. Li, Z. Li, T. C. Wang, J. T. Hupp, O. K. Farha, *Nat. Rev. Mater.* **2016**, *1*, 15018.
[84] T. Zhou, Y. Du, A. Borgna, J. Hong, Y. Wang, J. Han, W. Zhang, R. Xu, *Energy Environ. Sci.* **2013**, *6*, 3229.
[85] H. B. Wu, X. W. D. Lou, *Sci. Adv.* **2017**, *3*, eaap9252.
[86] H. Konnerth, B. M. Matsagar, S. S. Chen, M. H. Prechtl, F.-K. Shieh, K. C.-W. Wu, *Coord. Chem. Rev.* **2020**, *416*, 213319.
[87] J. Wang, Z. Huang, W. Liu, C. Chang, H. Tang, Z. Li, W. Chen, C. Jia, T. Yao, S. Wei, *J. Am. Chem. Soc.* **2017**, *139*, 17281.
[88] J. Wang, W. Liu, G. Luo, Z. Li, C. Zhao, H. Zhang, M. Zhu, Q. Xu, X. Wang, C. Zhao, *Energy Environ. Sci.* **2018**, *11*, 3375.
[89] W. Cheng, X. F. Lu, D. Luan, X. W. Lou, *Angew. Chem., Int. Ed.* **2020**, *59*, 18234.
[90] H. Zhang, G. Liu, L. Shi, J. Ye, *Adv. Energy Mater.* **2018**, *8*, 1701343.
[91] J. Zhang, H. Yang, B. Liu, *Adv. Energy Mater.* **2021**, *11*, 2002473.
[92] L. Zou, Y. S. Wei, C. C. Hou, C. Li, Q. Xu, *Small* **2021**, *17*, 2004809.
[93] Q. Zhang, J. Guan, *Adv. Funct. Mater.* **2020**, *30*, 2000768.
[94] Y. Yang, Y. Qian, H. Li, Z. Zhang, Y. Mu, D. Do, B. Zhou, J. Dong, W. Yan, Y. Qin, *Sci. Adv.* **2020**, *6*, eaba6586.
[95] L. Zhang, J. M. T. A. Fischer, Y. Jia, X. Yan, W. Xu, X. Wang, J. Chen, D. Yang, H. Liu, L. Zhuang, *J. Am. Chem. Soc.* **2018**, *140*, 10757.
[96] Y. Cheng, S. He, J. P. Veder, R. De Marco, S. z. Yang, S. Ping Jiang, *ChemElectroChem* **2019**, *6*, 3478.
[97] D. Zhang, L. Gong, J. Ma, X. Wang, L. Zhang, Z. Xia, *J. Phys. Chem. C* **2020**, *124*, 27387.
[98] L. Xu, D. Deng, Y. Tian, H. Li, J. Qian, J. Wu, H. Li, *Chem. Eng. J.* **2021**, *408*, 127321.
[99] X. Zhong, S. Ye, J. Tang, Y. Zhu, D. Wu, M. Gu, H. Pan, B. Xu, *Appl. Catal. B* **2021**, *286*, 119891.
[100] X. Zhu, D. Zhang, C.-J. Chen, Q. Zhang, R.-S. Liu, Z. Xia, L. Dai, R. Amal, X. Lu, *Nano Energy* **2020**, *71*, 104597.
[101] X. Zhu, C. Hu, R. Amal, L. Dai, X. Lu, *Energy Environ. Sci.* **2020**, *13*, 4536.
[102] L. Zhang, R. Si, H. Liu, N. Chen, Q. Wang, K. Adair, Z. Wang, J. Chen, Z. Song, J. Li, *Nat. Commun.* **2019**, *10*, 1.
[103] Y. Li, Q. Zhang, C. Li, H.-N. Fan, W.-B. Luo, H.-K. Liu, S.-X. Dou, *J. Mater. Chem. A* **2019**, *7*, 22242.
[104] S. Yuan, L. L. Cui, Z. Dou, X. Ge, X. He, W. Zhang, T. Asefa, *Small* **2020**, *16*, 2000742.
[105] Y. Qian, T. An, K. E. Birgersson, Z. Liu, D. Zhao, *Small* **2018**, *14*, 1704169.
[106] W. Ren, X. Tan, W. Yang, C. Jia, S. Xu, K. Wang, S. C. Smith, C. Zhao, *Angew. Chem., Int. Ed.* **2019**, *58*, 6972.
[107] Y. Kong, T. He, A. R. P. Santiago, D. Liu, A. Du, S. Wang, H. Pan, *ChemSusChem* **2021**, *14*, 3257.

Tianwei He received his Ph.D. degree in Physical Chemistry in 2020 from the Queensland University of Technology, Australia. He is currently working as a postdoctoral researcher at the Fritz Haber Institute of the Max Planck Society Berlin, Germany. He has published over 30 articles in very prestigious journals such as Journal of the American Chemical Society, Advanced Materials, Small Methods, Journal of Materials Chemistry A, and Nano Research. His research interest mainly focuses on computational discover and design catalysts that are active, efficient, selective, stable, and cheap which can ultimately enable large-scale applications.

Alain R. Puente Santiago received his Ph.D. degree in Physical Chemistry with distinction (July 2017) from the University of Cordoba, Spain. He is currently starting a new position as a postdoctoral researcher at the University of Texas at Austin, United States. He has published 57 publications in very prestigious journals such as Journal of the American Chemical Society, Angewandte Chemie, Renewable and Sustainable Energy Reviews, Journal of Materials Chemistry, Chemical Society Reviews A, and Green Chemistry. His research interests tackle the development of low-dimensional nanostructures for electrocatalytic, sensing, and energy storage applications.

Rafael Luque (Ph.D. in 2005 from Universidad de Cordoba, Spain) has significant experience in biomass and waste valorization practices to materials, fuels, chemicals, and nanoscale chemistry (500+ publications, h-index 70, 21 000 citations, 5 patents, 10 edited books). Prof. Luque is Editor-in-Chief of Molecular Catalysis and is serving in the Advisory/ Editorial Board of over 10 Q1 RSC, Wiley, ACS, and Elsevier Journals. Prof. Luque was named in 2018 and 2019 as Highly Cited Researcher and is Director of the Center for Molecular Design and Synthesis at RUDN University in Moscow, Russia, and Chair Professor at the Xi'an Jiaotong University.

Aijun Du received a Ph.D. from the Fudan University of China in 2002. He is currently a full Professor at the School of Chemistry and Physics in the Queensland University of Technology, Australia. His research lies at the interface of Chemistry, Physics, and Engineering, focusing on the design and development of innovative materials for energy, electronics, and environmental applications using advanced theoretical modeling approaches.

Hui Pan is a professor in the Institute of Applied Physics and Materials Engineering, and the founding head of the Department of Physics and Chemistry in the Faculty of Science and Technology at the University of Macau. He got his Ph.D. degree in Physics from the National University of Singapore in 2006. In his research, a combined computational and experimental method is used to design and fabricate novel nanomaterials for applications in energy conversion and storage (such as electrocatalysis, photocatalysis, water splitting, N2/CO2 reduction, supercapacitors, hydrogen storage, and fuel cells), electronic devices, spintronics, and quantum devices.